Geo-Mar Lett (2010) 30:47–62
DOI 10.1007/s00367-009-0152-8

ORIGINAL

A snapshot of suspended sediment and fluid mud occurrence in a mixed-energy embayment, Tijucas Bay, Brazil

Carlos Augusto França Schettini · Dermeval Costa de Almeida · Eduardo Siegle · Antônio Carlos Brandão de Alencar

Received: 2 October 2008 / Accepted: 17 July 2009 / Published online: 31 July 2009

Abstract Along the southern Brazilian coast, Tijucas Bay is known for its unique muddy tidal flats associated with chenier plains. Previous field observations pointed to very high suspended sediment concentrations (SSCs) in the inner parts of the bay, and in the estuary of the Tijucas River, suggesting the presence of fluid mud. In this study, the occurrences of suspended sediments and fluid mud were examined during a larger-scale, high-resolution 2-day field campaign on 1–2 May 2007, encompassing survey lines spanning nearly 80 km, 75 water sampling stations for near-bottom density estimates, and ten sediment sampling stations. Wave refraction modeling provided qualitative wave energy estimates as a function of different incidence directions. The results show that SSC increases toward the inner bay near the water surface, but seaward near the bottom. This suggests that suspended sediment is supplied by the local rivers, in particular the Tijucas. Near-surface SSCs were of the order of 50 mg l^{-1} close to the shore, but exceeded 100 mg l^{-1} near the bottom in the deeper parts of the bay. Fluid mud thickness and location given by densimetry and echo-sounding agreed in some places, although being mostly discordant. The best agreement was observed where wave energy was high during the campaign. The discrepancy between the two methods may be an indication for the existence of fluid mud, which is recorded by one method but not the other. Agreement is considered to be an indication of fluidization, whereas disagreement indicates more consolidation. Wave modeling suggests that waves from the ENE and SE are the most effective in supplying energy to the inner bay, which may induce the liquefaction of mud deposits to form fluid mud. Nearshore mud resuspension and weak horizontal currents result in sediment-laden offshore flow, which explains the higher SSCs measured in the deeper parts of the bay, besides providing a mechanism for fine-sediment export to the inner shelf.

C. A. F. Schettini (✉)
Instituto de Ciências do Mar,
Universidade Federal do Ceará (LABOMAR/UFC),
Av. da Abolição 3207, Meireles,
Fortaleza CEP 60165-081, Brazil
e-mail: guto.schettini@gmail.com

D. C. de Almeida
Mestrado em Ciência e Tecnologia Ambiental,
Centro de Ciências Tecnológicas da Terra e do Mar,
Universidade de Vale do Itajaí (CTTMar/UNIVALI),
R. Uruguai 458,
Itajaí, SC 88302-202, Brazil

D. C. de Almeida
Serviços de Operações Marítmas LTDA (SOMAR),
R. da Assembléia 11,
Rio de Janeiro, RJ 20011-001, Brazil

E. Siegle
Instituto Oceanográfico, Universidade de São Paulo (IO-USP),
Praça do Oceanográfico 191,
São Paulo, SP 05508120, Brazil

A. C. B. de Alencar
Centro de Ciências Tecnológicas da Terra e do Mar,
Universidade de Vale do Itajaí (CTTMar/UNIVALI),
R. Uruguai 458,
Itajaí, SC 88302-202, Brazil

Introduction

Mud is an important component in sedimentary environments and biogeochemical systems. It is a mixture of clayey cohesive sediments, non-cohesive particles (silt and sand), organic matter, water, and gas (e.g., CH_4 and H_2S),

which responds in a complex manner to hydrodynamic forcing agents such as waves and currents (Dyer 1986; Raudkivi 1990; van Rijn 1993; Winterwerp and van Kesteren 2004). Mud accumulation is a common feature in estuaries and on coastal plains where siltation of harbors (e.g., Winterwerp 2005) and/or coastal pollution (e.g., Menon et al. 2004) can be major concerns.

McAnally et al. (2007a, b) present an extensive review of the state of the art of fluid mud research in coastal areas. Fluid mud is defined as a suspension of cohesive sediments with concentrations exceeding the gel point, i.e., from 10 s to 100 s of grams per liter, resulting either from settling out of suspension, or from liquefaction of fine-grained deposits. Despite their fluid nature, such suspensions behave in a non-Newtonian way, can be mobile or stationary, and have thicknesses varying from a few centimeters to several meters (Winterwerp and van Kesteren 2004). Mobile fluid mud is viscous, and tends to flow downslope along the bed driven merely by gravity. Wright et al. (2001) emphasized that it is through gravity currents that most of the mud supplied by rivers to the inner shelf is moved to deeper waters.

Tijucas Bay is a unique environment along the south coast of Brazil, being the only embayment displaying extensive muddy intertidal areas (Buynevich et al. 2005). The mechanisms involved in fine-sediment trapping are still unclear. The hydrodynamics of the bay is forced by both tides and wind, and waves are therefore important near the shore. In addition, the Tijucas River, which discharges into the bay, contributes buoyancy effects. Due to this hydrodynamic complexity, it is difficult to affirm which of these driving agents dominates fine-sediment transport in this mixed-energy environment.

The Tijucas River is most probably the main source of fine sediments in the bay. During a preliminary hydrodynamic survey of the estuary in 2006, very high suspended sediment concentrations (SSCs) of the order of grams per liter were observed at the river mouth, as well as in the inner parts of the bay. In fact, an acoustic Doppler current profiler (ADCP) moored about 2 km upstream of the river mouth was completely buried in soft mud during its deployment. Fluid mud is usually observed in meso- and macrotidal estuaries where strong tidal currents resuspend bottom sediments that settle during slack water and/or neap tide periods, e.g., the Gironde in France (Allen et al. 1977), the Severn in England (Kirby and Parker 1983), and the Weser in Germany (Schrottke et al. 2006). In contrast to these, the Tijucas estuary is controlled by a microtidal regime with tidal currents of the order of 0.3 m s^{-1} (Schettini et al. 1996). The mean river discharge is of the order of 65 m^3 s^{-1}, which considering an average width of 150 m and a mean depth of 2 m, results in an average river flow velocity of about 0.2 m s^{-1}. The mean SSC in the estuary is of the order of only 70 mg l^{-1} (Schettini et al. 1996), which supports the contention that the physiography of the estuary prevents the development of significant waves due to short wind fetches. These observations suggest that, although the river catchments are the main source of the mud, the fluid mud observed in the estuary is not produced locally, but most probably along the adjacent shore from where it is advected back into the estuarine basin. Fluid mud may be produced by liquefaction of inner bay mud deposits due to wave action, from where it is advected into the estuary along the downslope gradient commencing from a depth of 1 m in the shallow river mouth to nearly 3 m a few km farther upstream.

The objective of this study was to test the conceptual reasoning outlined above, and to present a first assessment of suspended sediment and seabed properties in relation to wave energy dispersion in Tijucas Bay. Although the study provides only a snapshot of mud behavior in the bay, the results may help to improve our understanding of the evolution of the local chenier plains (Asp et al. 2005; Buynevich et al. 2005; Fitzgerald et al. 2005), and stimulate further research in the area.

Physical setting

Tijucas Bay is located in the central coastal sector of the State of Santa Catarina (Fig. 1), covering nearly 100 km^2. Length and width of the bay are of similar dimensions (each about 10 km). The northern headland near Porto Belo is formed by the Zimbros Peninsula, the southern flank by the rocky Ganchos headland. Both headlands have a high relief with hills reaching elevations of a few hundred meters. The inner bay is lined by extensive muddy intertidal areas bordered by a narrow coastal plain. The bay deepens gently in the offshore direction, the outer bay reaching a maximum depth of 15 m.

The regional climate is subtropical mesothermal wet, rainfall being uniformly distributed throughout the year in terms of monthly averages. The average precipitation is 1,415 mm $year^{-1}$, and the potential evapo-transpiration amounts to 900 mm $year^{-1}$. As a result, there is a positive annual hydrological balance. The average annual temperature is 21.4°C, minimum and maximum monthly averages being 17.3 and 26.0°C in August and February, respectively (GAPLAN 1986).

The total drainage area of the river basins bordering the bay extends over 2,800 km^2. The main river is the Tijucas, which has a catchment of 1,040 km^2 and debouches into the central sector of the bay (Fig. 1). From daily measurements since 1945 at a station at Major (gauge no. 84071000 of the Brazilian National Water Agency, ANA), the mean discharge of the Tijucas River is 24.4 m^3 s^{-1}. Another, small

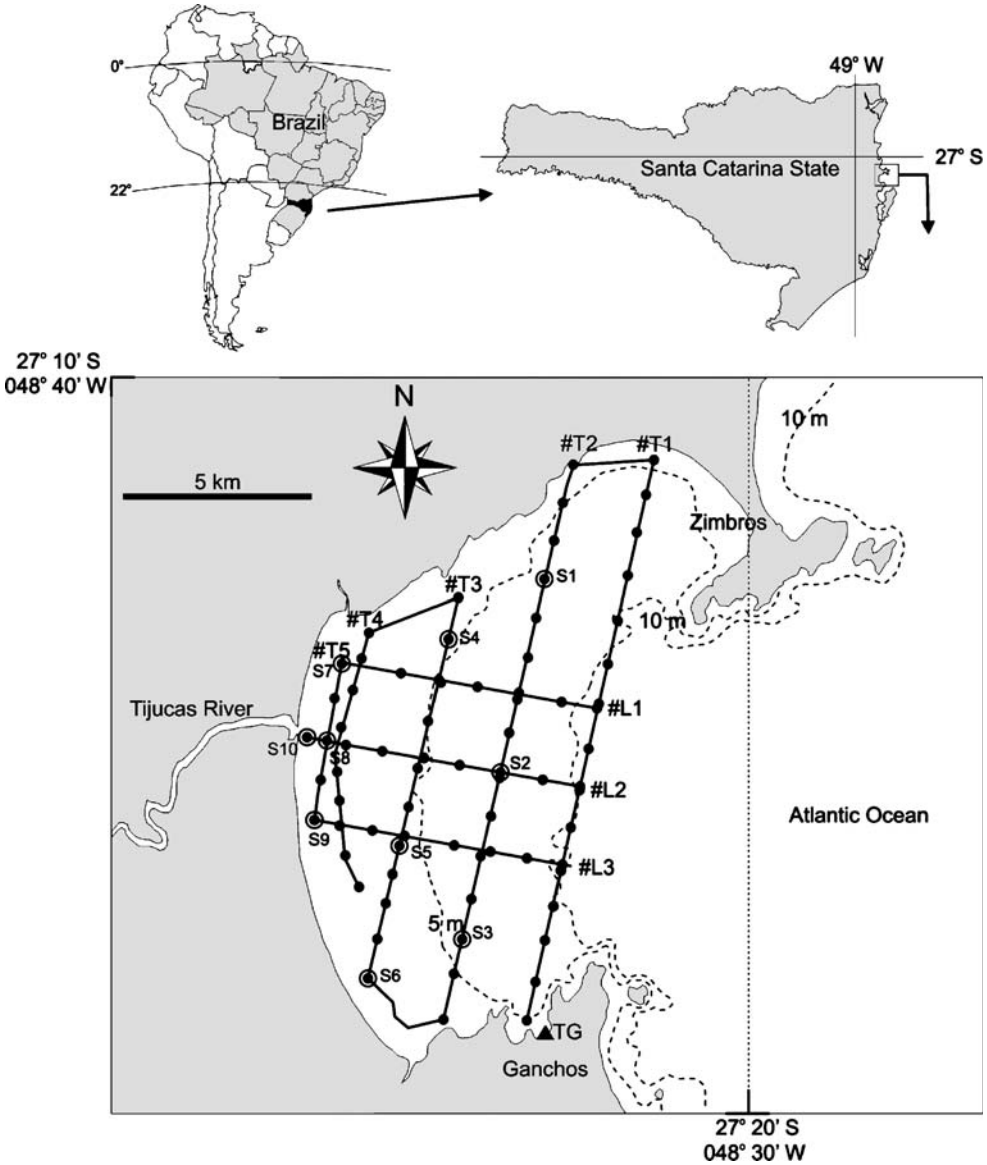

Fig. 1 Locality map of Tijucas Bay, showing the bathymetry, the locations of the transverse and longitudinal survey tracks (#Ti and #Li), the water column profiling sites (*closed circles*), and the bottom sample stations (*open circles*, Si). The *black triangle* (TG) indicates the location of the tide gauge station

stream, the Inferninho, which discharges into the southern bay (Asp et al. 2005), contributes smaller amounts. Linear extrapolation for the whole drainage area gives an estimated mean fluvial discharge of the order of 65 m^3 s^{-1} for the period 1945–2005. As in the case of other fluvial systems of Santa Catarina State, the fluvial discharge is highly variable on a daily basis. The relatively small drainage area means that runoff is rapid, being accomplished within a few hours. Sediment-laden floods are produced in the wake of cold fronts in winter and thunder storms in summer, lasting from several hours to a few days. Episodic high-discharge events are interrupted by long periods (weeks to months) of low discharge (Schettini 2002a).

The region has a microtidal regime, predominantly of the semidiurnal type with a mean tidal range of about 0.8 m, fluctuating from 0.3 m at neap to 1.2 m at spring tide (Schettini 2002a). Meteorological effects account for 30% of the variance in sea level, and extreme events associated with southerly winds generated during the passage of cold fronts can produce meteorologically forced tide levels exceeding 1 m (Truccolo et al. 2006).

The wave climate of the region is still poorly understood. The most detailed data available to date are those of Araújo et al. (2003), which have also been used as boundary condition in the simulations of Siegle and Asp (2007), based on 1-year-long records of wave measurements acquired at an offshore mooring (water depth 80 m) off Santa Catarina Island (27.75°S, 48.15°W). These authors identified five major wave systems for the southern coastal sector of Brazil: (1) a well-developed 8-s sea from the east, produced by winds of the South Atlantic anticyclonic system; (2, 3) swells of 11 and 14 s from the southeast; and (4, 5) minor transient wind-generated wave fields of variable directions associated with certain phases

of cold-front passages. Although the modal wave height is of the order of 1.5 m throughout the year, mean wave heights increase during winter. Unfortunately, this 1-year dataset did not include any extra-tropical events, locally known as 'lestada', which episodically produce very energetic wave conditions.

The Holocene evolution of the Tijucas coastal plain has recently attracted interest because of the unique set of cheniers and beach ridge systems (Asp et al. 2005; Buynevich et al. 2005; Fitzgerald et al. 2005; Hesp et al. 2009). The chenier plains are depositional features dominated by muddy sediments, the main source of the mud having been attributed to the Tijucas River. In comparative terms, the SSC in the Tijucas estuary is three times higher than that of other estuaries in the region. The mean SSC recorded in the Tijucas estuary over a tidal cycle at neap tide and low river discharge was 70 mg l^{-1}, whereas in the Itapocu (~70 km north) and Camboriú (~25 km north) estuaries it was 19 and 33 mg l^{-1} under the same conditions, respectively (Schettini et al. 1996). Interestingly, the name 'Tijucas' is a Portuguese version of 'Ty-Yuca', meaning 'black mud' in the native Tupy-Guarani language. Evidently, Tijucas Bay has a long-standing record of a mud-dominated environment.

Materials and methods

Fieldwork

The field campaign was designed to obtain high-resolution spatial information on the distribution of SSC and bottom characteristics in Tijucas Bay in the shortest possible period of time in order to provide a quasi-synoptic (snapshot) picture. Data on water levels, bathymetry, bottom sediment density, salinity, temperature, turbidity, suspended matter, and bottom sediment characteristics were therefore acquired during a single survey on 1–2 May 2007. Turbidity measurements were carried out by optical and acoustic methods, and converted into SSCs through calibration procedures.

Water level was monitored with a pressure tide gauge model TG-420 by RBR™ moored at a pier in the southern part of the bay (cf. Fig. 1), recording data at 10-minute intervals. The water-level time series was later used to match the measurements with the tidal phase in the course of the campaign, and to correct the bathymetric data.

The survey lines consisted of five transverse (#Ti) and three longitudinal transects (#Li) relative to the bay's main axis (Fig. 1). The survey was interrupted every 1 km to carry out vertical water profiling, collect water and bottom samples, measure bottom sediment density, and take sediment samples at selected stations. Navigation was by means of a D-GPS receiver (Navstar by Racal™). In all, the survey covered a distance of nearly 80 km, and encompassed 75 water column profiles with bottom density measurements, and ten sediment sampling stations.

Bathymetric echo-sounding, acoustic backscattering (ABS), salinity, temperature, and optical backscattering (OBS) were recorded continuously along the transect lines. Bathymetric dual-frequency soundings were performed by means of a Knudsen™ 320 M dual-frequency echo-sounder, operating at 210 and 33 kHz. ABS was recorded by means of an ADCP model ADP-1500 (Sontek™) deployed from a towed catamaran with an attached salinity, temperature, and turbidity recorder (CTD model SD-202, Saiv A/S™). The turbidity meter was a SeaPoint™ optical backscatter sensor wired to the CTD. The catamaran was towed alongside the boat to avoid interference of the propeller (bubbles) in the ABS records. Both the ADCP and CTD were programmed to record at 5-s intervals. The ADCP was configured to perform measurements with a vertical resolution of 0.5 m.

During the survey interruptions spaced at 1-km intervals, vertical profiles of salinity and temperature were recorded using an additional CTD (model SD-204, Saiv A/S™) fitted with an OBS (SeaPoint™). Near-bottom sediment density was measured with a densimeter of the type Densitune (Stema™). Surface water samples were collected for SSC determination, and bottom samples were collected with a Ponar-like grab sampler. Bottom sampling was restricted to ten stations (labeled S1, S2, etc., in Fig. 1).

Complementary data on wind speed and direction were obtained from a meteorological station situated at Itajaí, nearly 40 km north of Tijucas Bay. Since no river discharge data were available for the Tijucas drainage basin during the present study period, this was estimated via extrapolation of corresponding data for the neighboring Itajaí-Açu River obtained from the Brazilian Water Agency (Indaial fluviometric gauge station).

Suspended sediment measurements

SSC was derived from OBS (e.g., Downing et al. 1981) and ABS (e.g., Gartner 2004; Hoitink and Hoekstra 2005) measurements through calibration with suspended matter concentrations determined gravimetrically from water samples. It has become common practice to use SSCs derived from the ABS of commercially available ADCPs (e.g., Holdaway et al. 1999; Gartner 2004; Hoitink and Hoekstra 2005; Schettini and Zaleski 2006; Zaleski and Schettini 2006), although some problems, e.g., the contribution by acoustic noise, are still unresolved (Bartholomä et al. 2009). The main advantage of using the ABS, once calibrated, is its excellent water column coverage, and the possibility to obtain data continuously along the boat's track.

The water samples of 0.5 l were refrigerated after sampling until being processed in the laboratory. The

samples were filtered through membrane filters (Millipore™, 0.45 μm pore size), and the SSCs were recorded as dry sediment mass per unit volume of seawater. The SSCs from the water samples ranged from 5 to 75 mg l^{-1}, a reasonable span for OBS and ABS calibration in this case.

The OBS calibration was accomplished by cross-correlation between the instrument readings and the SSCs obtained from water samples. The relation intrinsically takes the effects of color and grain size into account. A direct linear relation was established for the present data. This is consistent with the findings of Kineke and Sternberg (1992), who showed that a linear correlation is valid up to several 100 s mg l^{-1}, whereas at higher concentrations the relation initially becomes nonlinear, and at SSCs of the order of 1,000 s mg l^{-1} the relation becomes inverse. The ABS calibration is necessary to correct the ADCP return signal strength from counts to acoustic intensity in decibels (dB). The normalization of the acoustic signal to compensate for attenuation effects with distance from the transducers, and the geometrical aperture of the beams is achieved through the sonar equation (Deines 1999; Lohrmann 2001; Gartner 2004)

$$\mathrm{ABS} = K_C(E - E_r) + 20\log_{10}(R) + 2\alpha_w(R) + \mathrm{TS} \quad (1)$$

where E is the echo intensity recorded in counts, which must be subtracted from the instrument noise level E_r, and converted into acoustic intensity in dB by the scale factor K_C. The second and third terms account for the two-way transmission loss, the second due to spreading, and the third due to absorption. R is the distance from the instrument, given by $Z/\cos\theta$ where Z is the distance from the transducer, and θ is the transducer angle from the vertical. α_w is the water absorption coefficient. TS is the target strength, which is a function of particle size and concentration in the water column. According to Gartner (2004), this term can be neglected for a 1,200-kHz frequency ADCP unless the particle size is very small (e.g., <10 μm) and/or concentration is very high (e.g., >1,000 mg l^{-1}). In the present case, the ADCP had a frequency of 1,500 kHz, SSC ranged from 10 s to 100 s mg l^{-1}, and particle size was unknown, although this can be considered to have been of the order of several 10 s to 100 s μm as reported for flocculated material (e.g., Eisma 1986). Thus, this last term was not considered in the ABS estimation.

Figure 2 presents the OBS and ABS calibration curves. For this, ten ADCP and CTD readings averaged over 50 s were selected. These can be considered as being nearly synoptic to the water samples, which were taken immediately after the boat was on station. The second cell of the ADCP beams, located about 1.7 m below the surface, was used for this purpose. The OBS measurements and the water samples were taken about 1 m below the surface. The SSC as a function of the OBS was linearly fitted (n=25, r^2=0.9299) by the relation

$$\mathrm{SSC(OBS)} = 3.21 + 3.35\,\mathrm{OBS} \quad (2)$$

and the SSC as a function of the ABS was best fitted (n=25, r^2=0.9416) by the relation

$$\mathrm{SSC(ABS)} = 0.1549\mathrm{ABS}^2 - 16.7\mathrm{ABS} + 454.1 \quad (3)$$

The redundancy of obtaining SSC distributions from both OBS and ABS is justified by the risk of the ABS calibration procedures. The ABS calibration needs to be performed in situ because of the large sampling volume. The success depends on whether a wide range of SSCs (10 s to 100 s mg l^{-1}) is available, and a rigorous synchronization between ADCP data and water sampling can be achieved. The main risk was that during the campaign the SSC range was too small for a reliable ABS calibration. Alternatively, OBS calibrations can be carried out in the laboratory by preparing a highly concentrated suspension using bulk sediment, and a stepwise dilution by adding known volumes of clear seawater.

Fluid mud measurements and sediment analysis

The measurement of fluid mud, both in spatial extent and in thickness, is still a complex task, mainly because of the ephemeral nature of the phenomenon, and the uncertainties in defining its upper and lower boundaries (Teeter 1994). Formerly, gamma-ray densimeters with pressure transducers were used as a way to determine the fluid density as a function of depth (McAnally et al. 2007a). However, the manipulation of such radioactive devices involves specially trained staff, rigid safety controls, and special environmental licenses. Vibrating-fork densimeters are an alternative method in which one leg of the tuning fork vibrates, while the response vibration frequency of the other leg is analyzed to produce a density estimation based on previous calibration using local sediments (McAnally et al. 2007b).

The calibration of the vibrating-fork densimeter is achieved by lowering the tuning fork into a bucket (~20 l) containing a water-sediment mixture, followed by the density calibration from the known volume and weight of material in the bucket. Stepwise addition of known water volumes to the mixture produces a gradient of successively lower densities. In this way, pairs of calculated densities and instrument readings are obtained, the calibration being performed by the software supplied by the manufacturer of the densimeter (Stema™). Once calibrated, the instrument is lowered at nearly constant speed (~0.5 m s^{-1}) through the water column until the bed is reached. At the same time, a

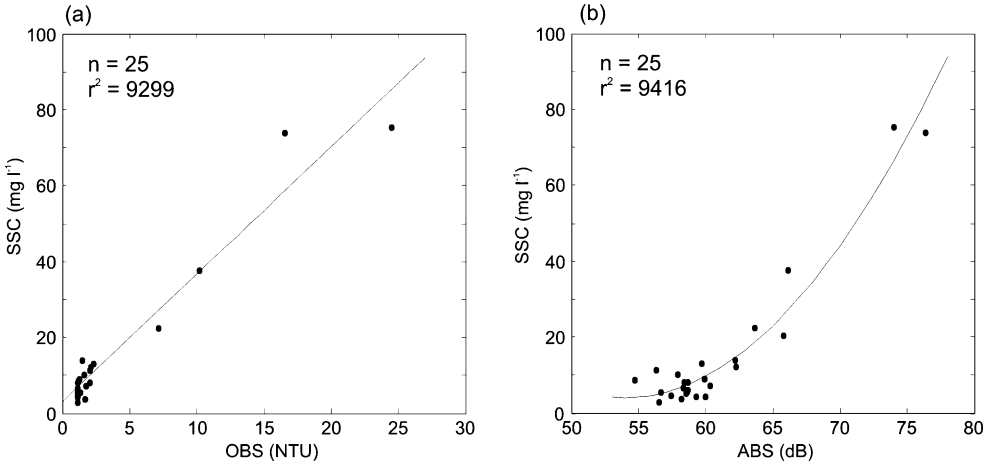

Fig. 2 **a** Calibration curves to convert optical backscatter (OBS, NTU), and **b** acoustic backscatter (ABS, dB) into suspended sediment concentration (SSC, mg l^{-1})

pressure transducer at the top of the instrument records the depth. The data acquisition rate was 10 Hz, enabling the identification of soft mud layers as thin as 10 cm. Fluid mud thickness was defined as the difference in depth between the 1,070 and 1,200 kg m^{-3} density levels. These values are, for example, used in standard hydrographic surveys by the Somar/Vanoord dredging company from whom the instrument was borrowed. A value of 1,200 km m^{-3} is commonly taken for the lower boundary, assuming that this indicates the change from mobile (fluid) to stationary (semi-consolidated) mud, although this is not necessarily always correct (Winterwerp and van Kesteren 2004). Figure 3 presents an example of a vertical density profile produced by the tuning-fork densimeter, suggesting the occurrence of a fluid mud layer and demonstrating that the above boundary conditions are well satisfied in the present case.

Fluid mud can also be assessed indirectly through bottom acoustic properties (Schrottke et al. 2006; McAnally et al. 2007a). A common usage in harbor regions is the inference of fluid mud on the basis of dual-frequency echo-sounding. The higher frequency is usually 200 or 210 kHz, the lower one 25 or 33 kHz. The higher-frequency signal is sensitive to low-density gradients, and usually records the first interface at which the fluid density exceeds a certain value. Strictly, this value needs to be determined by in situ calibration exercises that, in practice, are rarely done. In the presence of fluid mud, the lower-frequency sound penetrates into the soft sediment until a suitable density impedance is encountered, e.g., the compact sediment surface at the base of the fluid mud layer. Fluid mud thickness is then considered to be the difference between the two depths. The lower-frequency echo return is obviously a function of sediment rheological properties other than only density (Fontein and Wal 2006). Nevertheless, non-calibrated dual-frequency echo-sounding is widely used as a proxy for fluid mud detection, being complementary to direct methods (Teeter 1994). Very high resolutions have recently been achieved with calibrated multiple-frequency parametric echo-sounders (Schrottke et al. 2006). The advantage of dual- or multiple-frequency echo-sounding is the possibility of recording acoustic bottom characteristics continuously along the boat's track, whereas direct measurements must be performed with intrusive instrumentation, e.g., castings from a moving or moored boat (e.g., Stark and Wever 2009), or by towing an instrument sled over the bed (e.g., Teeter 1992). Figure 4 shows an analogue echo-sounder record along section #T2

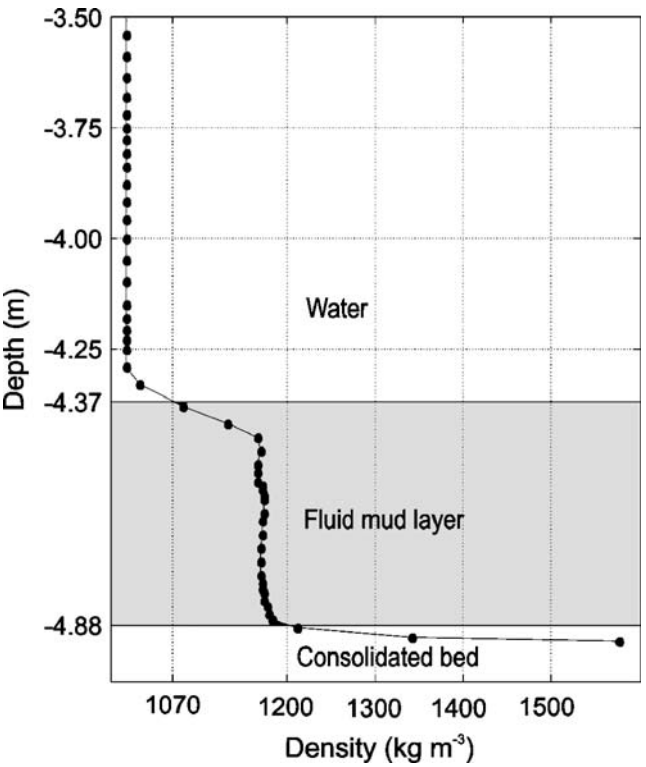

Fig. 3 Example of a vertical density profile (kg m^{-3}) across the water/fluid mud/consolidated bed interfaces produced by the tuning-fork densimeter

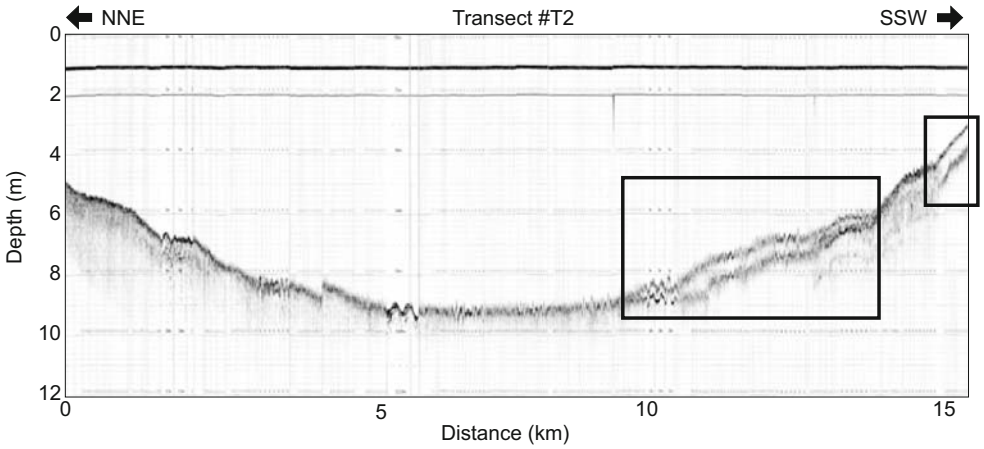

Fig. 4 Analogue record of combined 210- and 33-kHz soundings along the transverse transect #T2. The inset *rectangles* indicate 'transparent' mud sections in the southern part of Tijucas Bay revealed by double echoes produced by the traces of the two superimposed frequencies

of the study area, revealing a well-defined stretch of double-echo returns defining mud deposits.

Spatial distribution maps of fluid mud thicknesses and horizontal SSCs were generated by data interpolation on a regular grid using Matlab© (MathWorks Inc™), applying triangle-based linear interpolation over a 70×70 m grid. The final grid size was arbitrarily chosen based on visual inspection of resulting map qualities.

The bottom sediment samples were analyzed following standard procedures for determination of grain size, organic matter, and carbonate contents (e.g., Carver 1971). The coarse fractions (>63 μm) were sieved at 0.5-phi intervals, the fine fractions (<63 μm) analyzed by the pipette method. Clay is here defined as the <4 μm size fraction. Organic matter (OM) and carbonate contents were analyzed by combustion (Folk 1966; Dean 1974). In this paper, we present the sand/silt/clay ratios and OM contents only. Sediment data presentation and nomenclature follows Flemming (2000).

Wave modeling

The MIKE21 numerical model (developed by DHI Water & Environment) was used in order to define the wave energy distribution within Tijucas Bay. In this study, the MIKE21 wave module (SW) was applied to the wider Santa Catarina coast, with higher resolution for the Tijucas Bay area. MIKE21 SW is a spectral wave model that describes the propagation, growth, and decay of short-period waves (DHI 2007; also see Holthuijsen et al. 1989). This includes the effects of wave refraction and shoaling due to varying water depths, wave generation due to wind, and energy dissipation due to bottom friction and wave breaking.

The bathymetry used in the simulations was derived from the Brazilian Navy (DHN) nautical charts, the total model domain including a large area of the Santa Catarina shelf, covering 85 km north–south and 60 km offshore. The flexible mesh enables increased resolution in the region of interest. Since the aim of the wave simulations was to obtain information on the relative energy of the refracted waves across the bay, a wave of significant height H_s= 1.5 m and period T_s=8 s (cf. above) was propagated from offshore in seven incidence directions (NNE, NE, ENE, E, ESE, SE, SSE). In addition, wave predictions were extracted from the National Oceanic and Atmospheric Administration (NOAA) global wave prediction model (WAVEWATCH III—NWW3; Tolman 1997, 1999) for the offshore boundary of the wave refraction model (Fig. 5). Since there were no wave measurements available for the survey period, these data provided a best estimate of the wave conditions based on the NOAA meteorological data.

The wave-bottom interaction was assessed on the basis of the modeled radiation stress. The radiation stress is the mean momentum flux due to the presence of waves, being directly related to the dynamic pressure (generated by the waves). Refracted wave heights and radiation stresses were extracted along the 5-m depth contour to provide an estimate of wave energy dispersion in the bay. The model run was forced with the NWW3 hindcast wave data covering a 13-day period (20 April–3 May 2007), starting 10 days before the field campaign in order to reach

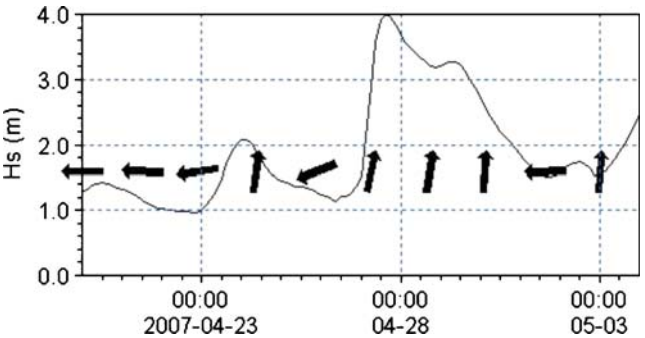

Fig. 5 Significant wave height (*line*) and direction (*arrows*) predicted by the WAVEWATCH III model for the offshore boundary of the Tijucas wave refraction model for the survey period

equilibrium in the modeled wave conditions. The wave data time series extracted from the NWW3 model shows increased offshore wave heights on the days preceding the field campaign (Fig. 5), with waves changing direction (from the southern quadrant) and reaching heights of up to 4 m.

Results

Environmental conditions

The weather during the field campaign was typical for the winter period in the region, with varying wind speed and direction due to the passage of a cold front. In the early hours of 1 May 2007, wind speed was of the order of 7 m s^{-1} from the southwest, changing to north after midday with decreasing wind speed. Early on 2 May, southwesterly winds blew at less than 4 m s^{-1}, increasing at noon to 8 m s^{-1}. During the week that preceded the campaign, the wind was mainly from the southwest, with short episodes of northerly winds, and variable speeds ranging from 2 to 8 m s^{-1}.

During the 2 weeks preceding the campaign, the discharge of the Tijucas River was of the order of 20 m^3 s^{-1}, except for 30 April when it increased to nearly 40 m^3 s^{-1}, a value persisting into early May at least. Compared to the historical data available (cf. above), the survey was carried out during a period of relatively low discharge, the average May discharge being about 50 m^3 s^{-1} for the period 1945–2005.

The vertical salinity and temperature profiles showed little variation during the campaign, with average values of 35.0±0.4 psu and 22.8±0.2°C, respectively. When pooling the vertical profile data with continuous surface datasets, the temperature-salinity (TS) diagram (Fig. 6a) reveals evidence of some scattering of temperature toward higher values, a trend attributed to the heating of water in the shallow parts of the bay in the course of the day. Slight scatter in salinity toward smaller values can be explained by short-lived increases in Tijucas River discharge. This is consistent with independent evidence of river runoff being relatively low at the time (cf. above), its effect being limited to the nearshore area south of the river mouth (Fig. 6b). Indeed, there is subtle evidence for a plume-like seaward isohaline trend in Fig. 6b.

Suspended sediments

Contrasting with the salinity and temperature distributions, the SSCs show strong horizontal and vertical gradients. Figure 7a–c illustrate the near-surface SSC distribution obtained from gravimetric analysis, and optical and acoustic measurements, respectively. These show good agreement in the distribution patterns as well as in the range of the values, thus strengthening our confidence in using the ABS as a proxy for SSC. The SSC values range from less than 10 to more than 50 mg l^{-1}, generally increasing toward the shore and toward the southern flank of the bay. Near-bottom SSC patterns, by contrast, are very different. In the shallow waters of the central inner bay, the near-bottom SSCs are about 20–35 mg l^{-1}, decreasing toward the sheltered parts of the bay in the rear of both headlands. Toward the offshore, the bottom SSCs initially decrease before rapidly increasing to values exceeding 100 mg l^{-1} (Fig. 7d). These data are based on the ABS of the ADCP measurements at about 1 m above the bottom.

The vertical distributions of SSC along the transverse (#T1, #T2 and #T3) and longitudinal (#L1, #L2 and #L3) transects are presented in Fig. 8. The highest SSCs were recorded near the seabed in the outer bay along transect #T1. However, there is a clear gradient from relatively high values in the south to very low values in the north off the

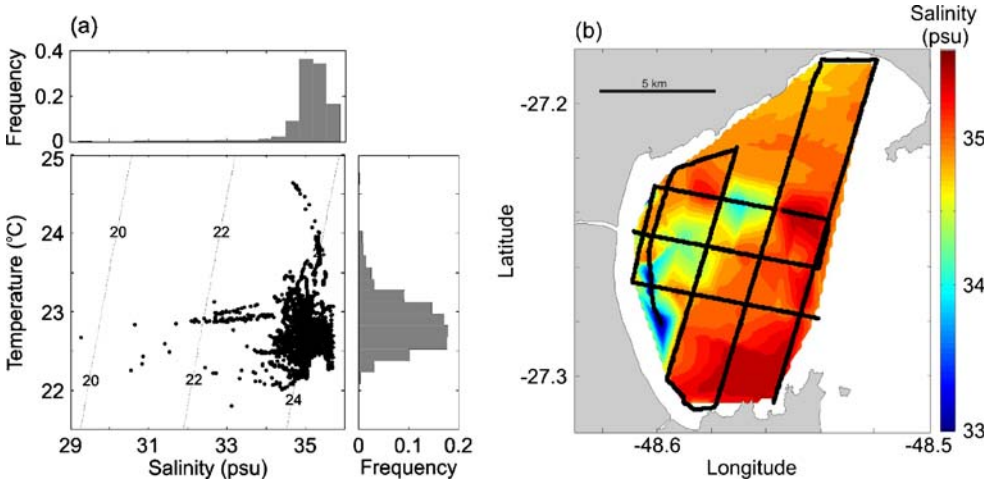

Fig. 6 **a** TS diagram of continuous surface and water column profiling data for Tijucas Bay, showing a temperature versus salinity plot with associated frequency histograms. **b** Map showing the distribution of sea-surface salinities

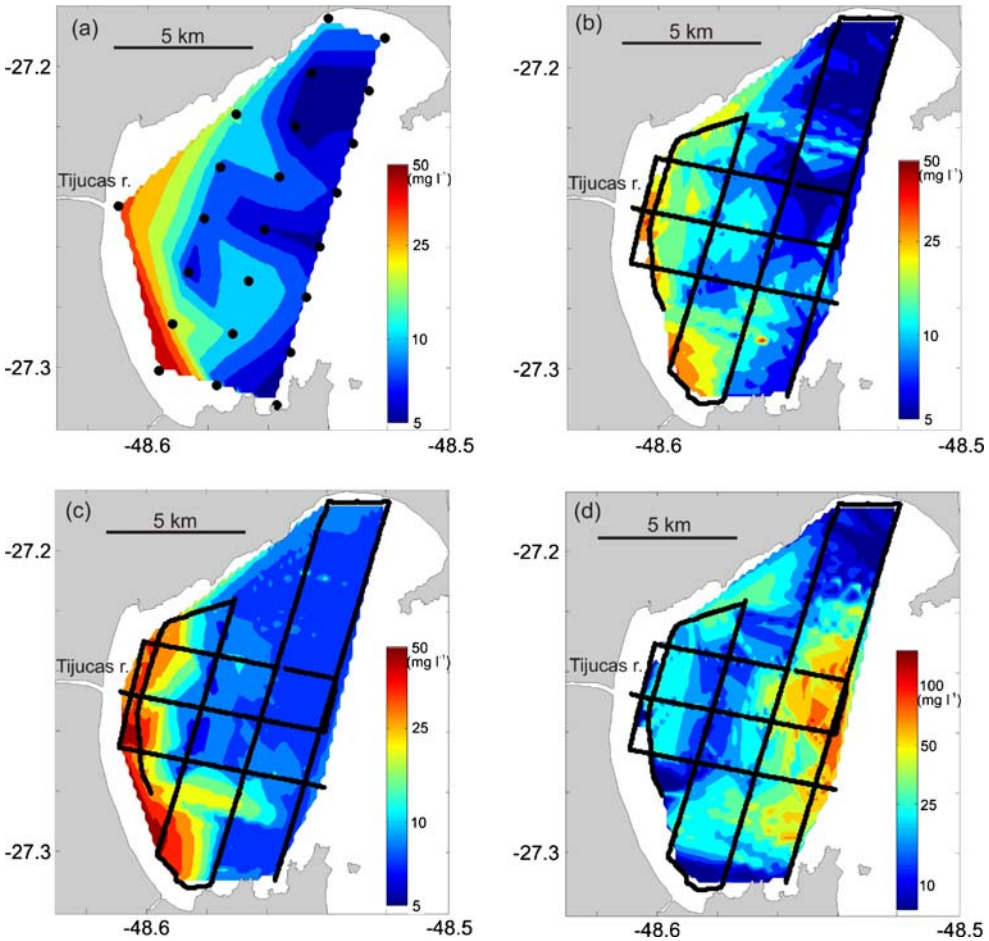

Fig. 7 Near-surface suspended sediment concentration (SSC, mg l^{-1}) obtained from **a** gravimetric analysis, and **b** acoustic and **c** optical measurements. **d** Near-bottom SSCs derived from acoustic measurements

Zimbros Peninsula. The pattern along transect #T2 is similar, although less well defined. Again the highest values are in the southern part of the bay, now extending through the entire water column. Furthermore, somewhat higher near-bottom SSC values than recorded along transect #T1 are also found in the northern part of the bay. In addition, there is a marked patch of low SSC values in the lower water column of the southern bay (Fig. 8a and b). This trend continues along #T3 where the SSCs reach relatively high values in the shallow parts of both the southern and the northern bay (Fig. 8c).

All three longitudinal transects reinforce the observations along the transverse transects, while adding greater detail along the depth gradient from inshore to offshore, both near the bottom and in the water column (Fig. 8d–f). Thus, all three transects show intermediate SSC values throughout the water column in the inner bay, followed by low values at intermediate depths, and high values in the lower water column of the outer bay. Noteworthy is the fact that the above trend is best developed along transect #L1 where the water column appears to be stratified with respect to SSC (Fig. 8d). The wedge of low SSC values at intermediate water depths seems to be a southwestward extension of the low SSC water body observed in the northern bay along transect #T1 (Fig. 8a). From this follows that, on the basis of the ABS records, the northern part of the bay appears to have been depleted in suspended sediment relative to the remainder of the bay at the time of the survey.

Bottom sediments

Although the low number of sediment samples precludes the generation of a sediment distribution map, the ternary diagram in Fig. 9 does reveal some subtle trends. Significantly, the highest sand contents are found in shallow water immediately off the Tijucas River mouth (samples S8 and S10), although even here the sediment consists of silty sandy mud, the sand content being <50%, and the silt content exceeding the clay content. Samples S5 and S6 from water depths <5 m in the southern bay consist of silty slightly sandy mud, the silt/clay ratios being similar

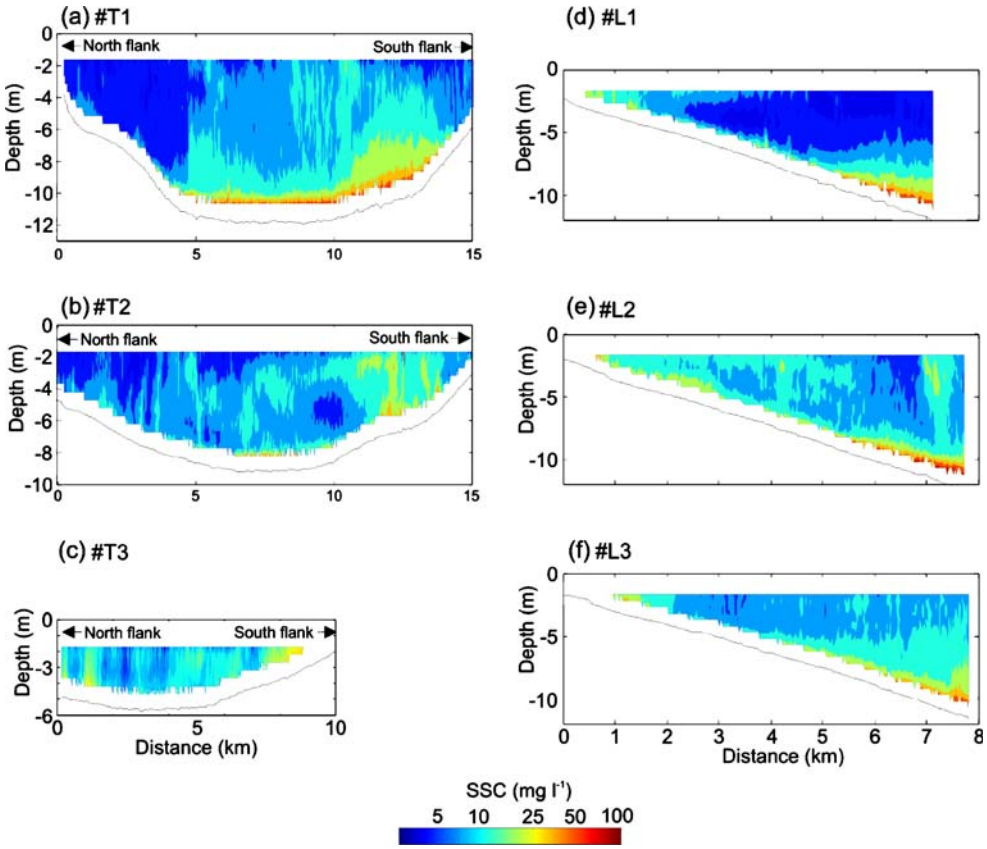

Fig. 8 Suspended sediment concentration (SSC, mg l^{-1}) along the transverse (**a**–**c**) and longitudinal (**d**–**f**) transects (cf. Fig. 1 for locations) derived from acoustic measurements

to those of samples S8 and S10. All other samples consist of plain mud with negligible sand contents. Of these, samples S1 and S4 comprise clayey silts, whereas the remainder (S2, S3, S7, and S9) consist of silty clays. The OM contents of the bulk sediments generally exceed 10%, and in some samples reach nearly 20%.

Fluid mud

The dual-frequency echo-soundings and the tuning-fork densimeter measurements both reveal the existence of fluid mud patches, albeit with considerable disagreement concerning thickness and partly also location. The densimetry measurements suggest a continuous fluid mud layer hardly thicker than 0.1–0.2 m covering the seabed of almost the entire bay (Fig. 10a). Thicker accumulations occur in the northern bay, near the shore in the central bay, and off the Ganchos headland in the south, and in deeper water of the outer bay. At these locations the densimeter suggests thicknesses of up to 0.4 m.

The echo-soundings, on the other hand, while also recording a thin fluid mud blanket over most of the bay, also reveal a number of distinct mud depocenters with thicknesses reaching at least 0.7 m (Fig. 10b). The largest of these (>10 km^2) is located offshore in the southern part of the bay. A second one is located off the Ganchos headland in the south. Both are clearly delimited on the echo-sounder trace in Fig. 4, but neither correlate with the densimeter records. A third depocenter is located near the shore of the central bay, here more or less coinciding with the densimeter measurements. The echo-sounder, on the other hand, failed to

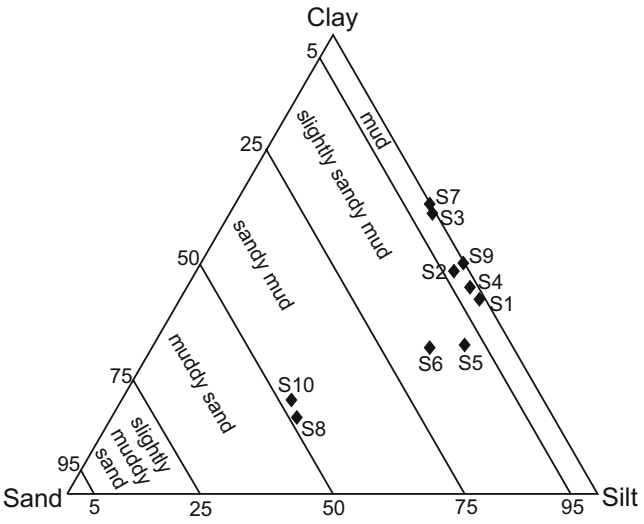

Fig. 9 Ternary diagram of sand/silt/clay ratios for Tijucas Bay bottom samples

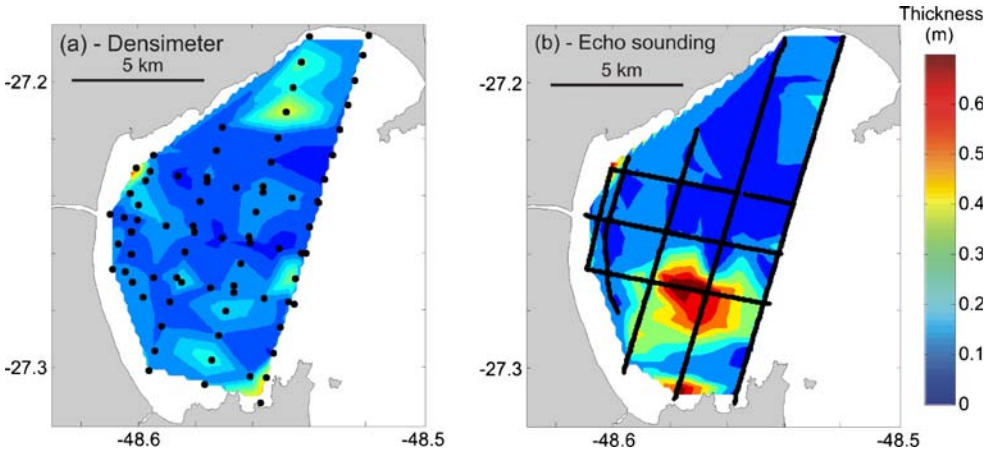

Fig. 10 Thickness of fluid mud (m) in Tijucas Bay, based on **a** tuning-fork densimeter measurements, and **b** dual-frequency echo-sounding

detect the thicker fluid mud patch recorded by the densimeter in the northern bay.

Wave energy

Figure 11 presents the modeled wave radiation stresses (colors), wave heights (arrow lengths), and directions (arrow orientation) for a wave of H_s=1.5 m and T_s=8 s, but for varying incident directions propagating into the bay. Purple indicates low wave energy, whereas lighter yellow tones indicate higher energy levels. As expected, waves from the east supply most energy to the inner bay. The energy decreases as the wave direction rotates northward or southward. Nevertheless, southward rotations produce more energy than do corresponding northward rotations. This trend is highlighted by the mean radiation stresses along the 5-m isobath for the different wave directions (Fig. 12).

In order to evaluate the simulations based on the NWW3 wave data for the survey period, the significant wave height and radiation stresses along the 5-m isobath were averaged for a period of 3 days (30 April to 2 May 2007), corresponding to the mean wave conditions in the bay during the survey period (Fig. 13). The diagram clearly shows that higher energy levels occurred from the center of the bay toward the northern headland, associated with an almost constant wave height of about H_s=0.6 m. From the center of the bay toward the southern headland, the energy decreases progressively to about 25% of its maximum, while H_s decreases by 50%. These results reflect the effect of the southerly winds at the time of the survey, which directed more wave energy toward the northern bay.

Discussion and conclusions

Once delivered to the coastal zone via river mouths, fine sediments enter a cycle of erosion, transport, and deposition until reaching deeper waters where the timescale for sediment remobilization increases (Wright and Nittrouer 1995). Near river mouths, the accumulation of fine sediments is most pronounced during periods of high river discharge and low-energy conditions in the nearshore (e.g., Traykovski et al. 2000). Eventually, the energy supplied by waves in conjunction with currents (geostrophic, tidal, or wind-driven) will segregate mud and sand. Sand is fed to the beaches and the upper shorefaces, whereas mud is carried into deeper waters, or toward the shore if tidal flats are developed. This simple concept incorporates several forcing parameters such as the magnitude of waves and currents, the regional coastal physiography, and the type and magnitude of sediment supply. Tijucas Bay is a semi-sheltered water body where mud is being trapped, and because of its particular physiography, intertidal mud flats are formed even under the microtidal regime and relatively high wave-energy levels (Asp et al. 2005; Buynevich et al. 2005). A conceptual model reflecting the hydraulic mechanisms responsible for trapping mud is beyond the scope of the present study, although the detailed ‘snapshot’ provided by the distribution of near-bottom mud and SSC in the bay does contribute toward such a model by showing that the bottom material is made of easily erodable, soft mud.

The Tijucas River is most probably the main source of mud in the bay, although its precise contribution is currently unknown. Nevertheless, in a comparative study of four estuaries in the region, the SSC of the Tijucas estuary was four times higher than that of the other estuaries under the same tidal and hydrological conditions (Schettini et al. 1996). This suggests a higher sediment discharge for the Tijucas than for the neighboring rivers, the difference being a function of the different size and geology of the drainage basin (Hesp et al. 2009). During the present study period, the fluvial discharge was rather low, and no measurable relation between salinity and SSC was observed. Indeed, the nearshore SSC was relatively high throughout the inner bay, there being no distinctive signature near the estuary mouth, as would be expected in

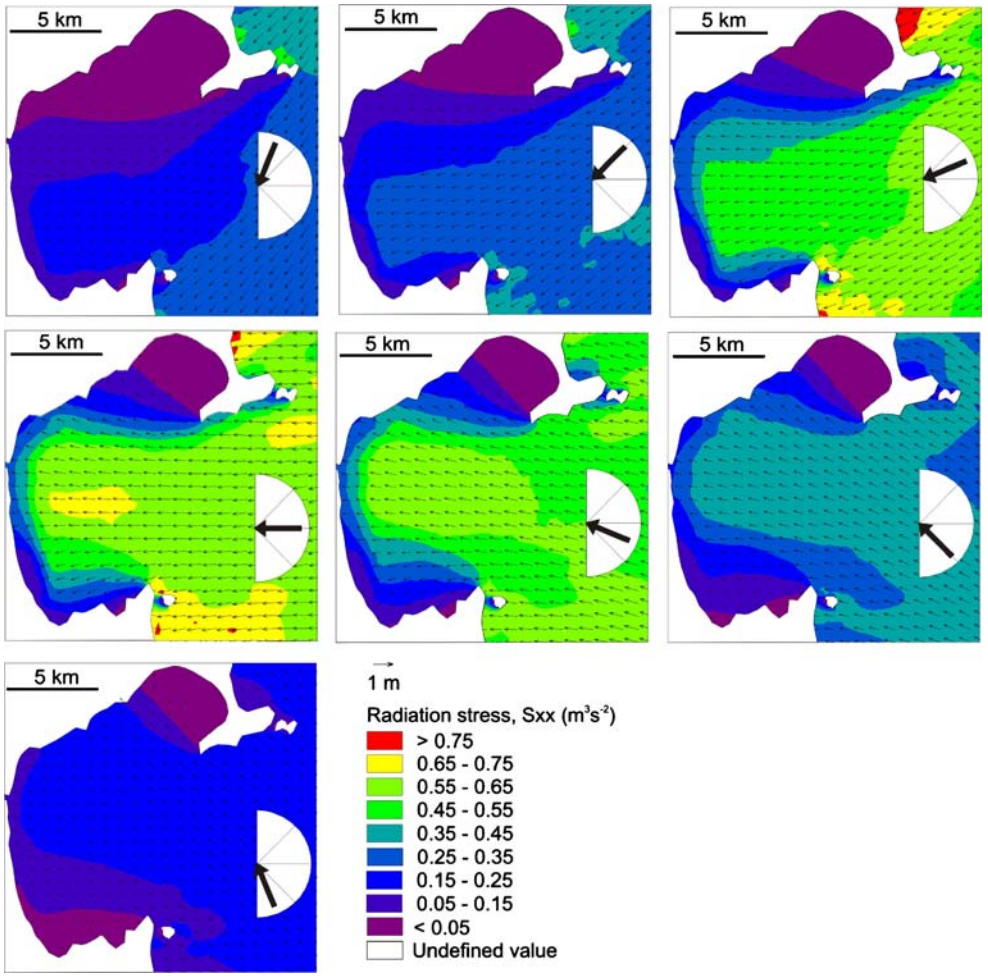

Fig. 11 Distribution of wave radiation stresses based on modeling at different angles of incidence

the case of significant river supply (Figs. 6, 7a–c). Therefore, considering that the estuarine dynamics of the Tijucas is similar to that of other estuaries in the region, as demonstrated for the Itajaí-Açu estuary (e.g., Schettini 2002a), the delivery of mud to the coast would take place in short episodic events of high discharge when river flow and sediment load can increase by two orders of magnitude (Schettini 2002b; Schettini and Toldo 2006). During periods of low river discharge, the estuary would act as a sediment trap for riverine material, even importing materials from the adjacent shelf (Schettini et al. 2006; Siegle et al. 2009).

Mud accumulation in Tijucas Bay is a long-term process, much longer than the more dynamical timescale of hours to months covered in the present study. This is well reflected in the mud-rich facies characterizing the Tijucas coastal plain (Buynevich et al. 2005; Hesp et al. 2009). Another fact indicating low mud export from the bay to the adjacent shelf, or alternatively a high trapping efficiency (e.g., Dyer 1995), are the very low SSCs observed in the shelter of both the northern and the southern headlands of the bay. These areas are popular tourist resorts offering tours to local clear-water diving spots.

Nevertheless, full understanding of mud dynamics in coastal environments requires measurements of many variables, some of which are difficult (if at all possible) to implement at appropriate temporal and spatial resolution. The present dataset provides undisputable evidence that (1) fluid mud occurs in Tijucas Bay, although there is considerable disparity between the applied methods (echo-sounding versus densimetry), and (2) the occurrence of fluid mud is not directly related to the distribution of near-bed SSC. Despite the lack of direct measurements of wave heights, currents, and river solid and liquid discharges during the study period, the findings suggest that the fluid mud is essentially produced by wave-induced liquefaction, rather than by settling from suspension, because in the latter case one would have expected a better relation between the distribution patterns of higher SSC values and the fluid mud patches.

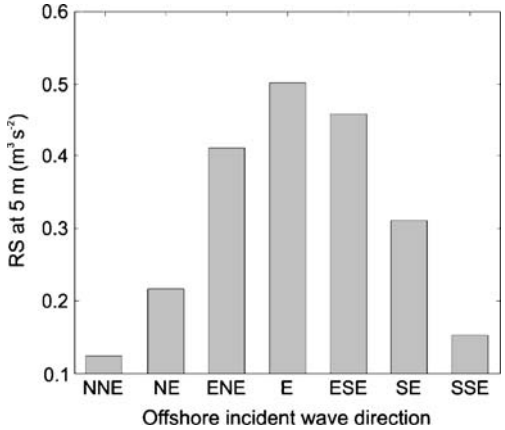

Fig. 12 Variation of radiation stress (RS) at 5 m depth as a function of incident wave direction from the offshore

The discrepancy between the two methods is not immediately understandable, although the most plausible explanation would be that the densimeter actually penetrated the fluid mud at all locations, and thereby recorded its true thickness. This would mean that the echo-sounder in some locations shows more than only fluid mud, the thicker 'transparent' deposits (cf. Fig. 4) evidently comprising semi-consolidated mud (>1,200 kg m^{-3}) that the densimeter could not penetrate. Conversely, the patch of greater fluid mud thickness recorded by the densimeter in the central northern bay, but which the echo-sounder failed to identify, would suggest that the fluid mud at this location must have been near its low-density limit (1,070 kg m^{-3}), and to which the 200-kHz frequency of the echo-sounder did not respond. It should be recalled here that, while the densimeter correctly delimited the fluid mud in the example illustrated in Fig. 3, no such calibration was available for the dual-frequency echo-sounder. This raises the question as to the reliability of non-calibrated echo-sounders to accurately detect fluid mud. In the present case, it would appear that the response of the 200-kHz frequency lies somewhere between the defined upper- and lower-density limits of fluid mud. The solution to this problem would obviously be to also calibrate the dual-frequency echo-sounder, or to use a multiple-frequency parametric echo-sounder of the type described in Schrottke et al. (2006).

The results of this study therefore suggest that the thicker mud patches were evidently in different stages of liquefaction or consolidation, each stage having a different rheology, and hence a different response of the echo-sounder to the local thixotropic state of the mud. Winterwerp and van Kesteren (2004) provide an example of this process in Rotterdam Harbor, where two echo-sounding observations were carried out at the same site, but at different times. On both occasions a fluid mud layer was recorded, but with a different vertical density structure in each case. In the present case, the dataset is merely a single snapshot, which does not enable an assessment of the temporal evolution of the feature.

The results of this study are also in good accordance with the southerly waves observed during the campaign, the energy dispersion of which was simulated by the wave

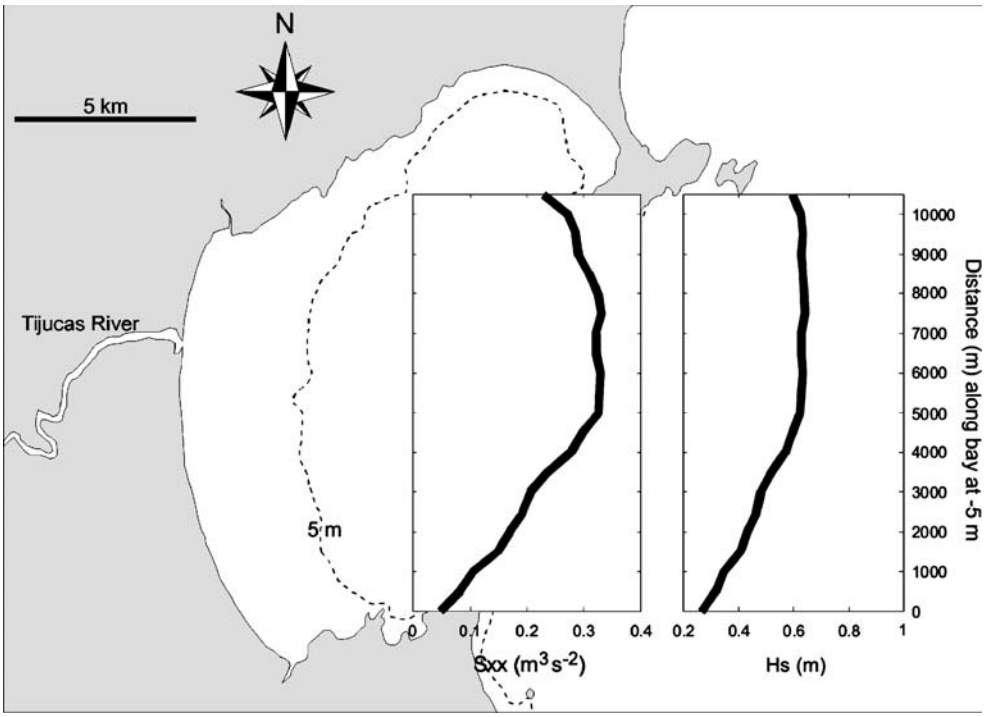

Fig. 13 Along-bay radiation stress (Sxx) and significant wave height (Hs) averaged for refracted waves at −5 m from 30 April to 3 May 2007, based on predicted offshore boundary conditions (WAVEWATCH III)

model. Cold fronts in southern Brazil have a recurrence time of 6 to 11 days, and usually last for 2 or 3 days (Stech and Lorenzzetti 1992). During their passage, the wind rotates from NE to SW or S. Under wave action, fluidization takes place, which produces, sustains, or even thickens fluid mud (e.g., Foda et al. 1993; de Wit and Kranenburg 1997; Lamb and Parsons 2005). The resistance to erosion of aggregated fine sediment particles will break down once sufficient shear stress acts on the bed. This can be achieved by strong unidirectional currents, or by wave action. The oscillatory pressure variations under waves result in periodically increased pore-water pressures, which are amplified resonantly with increasing liquefaction (Foda and Tzang 1994). After an initial strong rise in pore-water pressure, the pressure decays gradually as liquefaction and particle break-up progress (de Wit and Kranenburg 1997). This thixotropic behavior leads to progressive liquefaction of a mud layer, the thickness of the resulting fluid mud being dependent on the scale of the forcing. Once wave activity ceases, the mud enters a consolidation phase during which pore water is expelled. Under calm weather conditions this consolidation process can take a few days (e.g., Been and Sills 1981), but it will take longer under more variable energy conditions. During consolidation, the wet bulk density increases gradually, and may even result in the formation of several, vertically stacked layers with downward-increasing density. Such density discontinuities may produce acoustic impedances that echo-sounders may record, even at densities higher than 1,200 kg m^{-3} (e.g., Schrottke et al. 2006).

According to Winterwerp and van Kesteren (2004), two categories of suspended sediments can be distinguished: (1) low-concentration mud suspensions (LCMS), and (2) high-concentration mud suspensions (HCMS). The former usually has values of several 10 s mg l^{-1}, the latter of several 100 s to 1,000 s mg l^{-1}. Fluid mud would represent a third category with concentrations of 10 s to 100 s g l^{-1}. This wide range in concentrations makes it difficult to use a single technique to measure the complete spectrum of expected values, except if based on standard water (or core) sampling, and subsequent gravimetric analysis. However, this latter approach is extremely time-consuming, which severely limits the amount of data that could be obtained during a single survey. Although unable to accurately measure high SSCs close to the bed, as well as being unable to identify the transition to fluid mud, suspended sediment distributions derived from calibrated ADCP records have proven to be a useful approach in the present study where the main aim was to obtain continuous spatial records.

Tijucas Bay in general is a low-energy hydrodynamic environment, currents being driven mostly by wind, rather than by tides. The liquefaction of muddy bottom sediments and the formation of fluid mud are thus due mainly to wave action. Here, we considered wave radiation stress as an indicator of wave energy levels. Wave refraction simulations have shown that waves incident from the southern quadrant produce higher energy levels than those from the northern quadrant. This is due to the morphological configuration of the bay, which is protected from northern waves by the Zimbros headland, i.e., the bay is more exposed to waves approaching from the E and ESE. A similar pattern was observed when propagating waves predicted for the offshore region (cf. NWW3 model) during the survey period. Although preceded by storm waves from the south, the smaller waves propagating from the east would have resulted in higher energy levels within the bay. Considering the regional wave climate, wave energy distribution is dominated by waves from the E, SE, and S, which contribute over 90% to the wave frequency spectrum (Araújo et al. 2003). This would have led to a focusing of higher wave energy in the central part of the bay, coinciding with the observed fluid mud patches.

Localized fluid mud formation can lead to turbidity currents, one possible mechanism of removing sediments from the bay under favorable hydrodynamic conditions (e.g., Traykovski et al. 2000; Wright et al. 2001). Alternatively, mass entrainment would produce LCMS and HCMS, which would be more effectively advected by tidal or wind-induced currents on shorter timescales (Mehta et al. 1989). Therefore, increasing SSCs will also be associated with buoyancy effects and sediment-laden flows. The sediment-induced buoyancy effects already become manifest at moderate SSCs of the order of 10 s mg l^{-1} (Winterwerp and van Kesteren 2004). This is likely to have taken place in Tijucas Bay during the survey of early May 2007, as indicated by the increasing near-bed concentrations in the deeper parts of the bay. Despite the fact that most wave energy is dissipated at depths >5 m, wave energy will still be transferred to the muddy coast where Stokes' drift or wave-induced currents can be involved in the accumulation of muddy sediments near the shore. Considering the existence of low-intensity currents near the shore and near the bed, buoyancy effects will thus prevail and promote the transfer of sediment-laden flows to deeper waters.

Acknowledgements We are grateful to HIDROTOPO for kindly lending us the survey boat *Hidrotopo*, to SOMAR Ltd. for lending us the densimeter and the echo-sounder, to Marçal Duarte Pereira for his help during the survey, and to the anonymous reviewers and GML editors whose comments and suggestions greatly improved the manuscript. This study was funded by the Brazilian Research Council (CNPq) through the project TRANSEST: Sediment Transport in River Dominated Estuaries (No. 480851/2004-2); CNPq grants 306217/2007-4 (CAFS) and 308303/2006-7 (ES).

References

Allen GP, Sauzay G, Castaing P, Jouanneau JM (1977) Transport and deposition of suspended sediment in the Gironde estuary, France. In: Wiley M (ed) Estuarine processes, vol 2. Academic, New York, pp 63–81

Araújo CES, Franco D, Melo E, Pimenta F (2003) Wave regime characteristics of the southern Brazilian coast. In: Proc 6th Int Conf Coastal and Port Engineering in Developing Countries, COPEDEC VI, September 2003, Colombo, Sri Lanka, Paper no 97, CD-ROM

Asp NE, Buynevich I, Siegle E, Fitzgerald D, Klein AHF, Cleary W, Angulo R (2005) Coastal geomorphology of Tijucas, SC-Brazil: preliminary Holocene evolution model. In: Anais X Congr Associação Brasileira de Estudos do Quaternário, 9–16 October 2005, Guarapari, Brazil, ABEQUA, pp 6–12

Bartholomä A, Kubicki A, Badewien TA, Flemming BW (2009) Suspended sediment transport in the German Wadden Sea—seasonal variations and extreme events. Ocean Dynamics 59:213–225

Been K, Sills GC (1981) Self weight consolidation of soft soils: an experimental and theoretical study. Geotechnique 31:519–535

Buynevich I, Asp N, Fitzgerald D, Cleary W, Klein AHF, Siegle E, Angulo R (2005) Mud in the surf: nature at work in a Brazilian bay. EOS Trans Am Geophys Union 86:301–308

Carver RE (1971) Procedures in sedimentary petrology. Wiley, New York

Dean WE (1974) Determination of carbonate and organic matter in calcareous sediments and sedimentary rocks by loss on ignition; comparison with other methods. J Sediment Res 44(1):242–248

Deines KL (1999) Backscatter estimation using broadband acoustic Doppler current profilers. In: Proc IEEE 6th Work Conf Current Measurements, 13–16 September 1999, San Diego, CA, pp 249–253

de Wit PJ, Kranenburg C (1997) The wave induced liquefaction of cohesive sediment beds. Estuarine Coastal Shelf Sci 45:261–271

DHI (2007) MIKE21 FM. User guide and reference manual. DHI, Hørsholm

Downing JP, Sternberg RW, Lister CRB (1981) New instrumentation for the investigation of sediment suspension processes in the shallow marine environment. Mar Geol 42:19–34

Dyer KR (1986) Coastal and estuarine sediment dynamics. Wiley, New York

Dyer KR (1995) Sediment transport processes in estuaries. In: Perillo GME (ed) Geomorphology and sedimentology of estuaries. Elsevier, New York, pp 423–449

Eisma D (1986) Flocculation and de-flocculation of suspended matter in estuaries. J Sea Res 20(1/3):183–199

Fitzgerald DM, Cleary WJ, Buynevich IV, Hein CJ, Klein AHF, Nils EA, Angulo R (2005) Strand plain evolution along the southern coast of Santa Catarina, Brazil. J Coastal Res SI 50:1–15

Flemming BW (2000) A revised textural classification of gravel-free muddy sediments on the basis of ternary diagrams. Cont Shelf Res 20:1125–1137

Foda MA, Tzang SY (1994) Resonant fluidization of silty soil by water waves. J Geophys Res 99:463–475

Foda MA, Hunt JR, Chou HT (1993) A nonlinear model for the fluidization of marine mud by waves. J Geophys Res 98:7039–7047

Folk RL (1966) A review of grain-size parameters. Sedimentology 6 (2):73–93

Fontein W, Wal J (2006) Assessing nautical depth efficiently in terms of rheological characteristics. In: Proc Int Hydrographic Conf, 6–9 November 2006, Antwerp, Belgium, Hydro International

GAPLAN (1986) Atlas de Santa Catarina. Aerofoto Cruzeiro, Rio de Janeiro

Gartner JW (2004) Estimating suspended solid concentrations from backscatter intensity measured by Doppler current profiler in San Francisco Bay, California. Mar Geol 211:169–187

Hesp PA, Giannini PCF, Martinho CT, Silva GM, Asp NE (2009) The Holocene barrier systems of the Santa Catarina coast, southern Brazil. In: Dillenburg S, Hesp P (eds) Geology and geomorphology of Holocene coastal barriers of Brazil. Lecture Notes in Earth Sciences, vol 107. Springer, Berlin, pp 93–133

Hoitink AJF, Hoekstra P (2005) Observations of suspended sediments from ADCP and OBS measurements in a mud-dominated environment. Coastal Eng 52:103–118

Holdaway GP, Thorne PD, Flatt D, Jones SE, Prandle D (1999) Comparison between ADCP and transmissometer measurements of suspended sediment concentration. Cont Shelf Res 19:421–441

Holthuijsen LH, Booij N, Herbers THC (1989) A prediction model for stationary, short-crested waves in shallow water with ambient current. Coastal Eng 13:23–54

Kineke GC, Sternberg RW (1992) Measurements of high concentrated suspended sediments using the optical backscatterance sensor. Mar Geol 108(3/4):253–258

Kirby R, Parker WR (1983) The distribution and behavior of the fine sediment in the Severn estuary and inner Bristol Channel. Can J Fish Aquat Sci 40:83–95

Lamb MP, Parsons JD (2005) High-density suspensions formed under waves. J Sediment Res 75(3):386–397

Lohrmann A (2001) Monitoring sediment concentration with acoustic backscattering instruments. Nortek AS, Rud, Norway, Nortek Tech Note no 03

McAnally WH, Friedrichs C, Hamilton D, Hayter E, Shrestha P, Rodriguez H, Sheremet A, Teeter A (2007a) Management of fluid mud in estuaries, bays, and lakes. I. Present state of understanding of character and behavior. J Hydraul Eng 133 (1):9–22

McAnally WH, Teeter A, Schoellhamer D, Friedrichs C, Hamilton D, Hayter E, Shrestha P, Rodriguez H, Sheremet A, Kirby R (2007b) Management of fluid mud in estuaries, bays, and lakes. II. Measurement, modeling, and management. J Hydraul Eng 133 (1):23–38

Mehta AJ, Hayter EJ, Parker WR, Krone RB, Teeter AM (1989) Cohesive sediment transport. 1. Process description. ASCE J Hydraul Eng 115:1076–1093

Menon MG, Gibbs RJ, Phillips A (2004) Accumulations of muds and metals in the Hudson River estuary turbidity maximum. Environ Geol 34(2/3):214–222

Raudkivi AJ (1990) Loose boundary hydraulics, 3rd edn. Pergamon, New York

Schettini CAF (2002a) Caracterização física do estuário do rio Itajaí-Açu. Rev Brasileira Recursos Hídricos 7(1):123–142

Schettini CAF (2002b) Near bed sediment transport in the Itajaí-Açu River estuary, southern Brazil. In: Winterwerp JC, Kranenburg C (eds) Fine sediment dynamics in the marine environment. Elsevier, New York, pp 499–512

Schettini CAF, Toldo EE Jr (2006) Fine sediment transport modes in the Itajaí-Açu estuary, Southern Brazil. J Coastal Res SI 39:515–519

Schettini CAF, Zaleski AR (2006) A utilização de perfiladores acústicos de corrente por efeito Doppler na determinação do material particulado em suspensão na água: aplicações. Rev Brasileira Recursos Hídricos 11(2):201–208

Schettini CAF, Carvalho JLB, Jabor P (1996) Comparative hydrology and suspended matter distribution of four estuaries in Santa Catarina State, southern Brazil. In: Proc Worksh Comparative Studies of Temperate Coast Estuaries, 29 July–2 August 1996, Bahia Blanca, Argentina, IADO, pp 29–32

Schettini CAF, Ricklefs K, Truccolo EC, Golbig V (2006) Synoptic hydrography of a highly stratified estuary. Ocean Dynamics 56:308–319

Schrottke K, Becker M, Bartholomä A, Flemming BW, Hebbeln H (2006) Fluid mud dynamics in the Weser estuary turbidity zone tracked by high-resolution side-scan sonar and parametric sub-bottom profiler. Geo-Mar Lett 26(3):185–198. doi:10.1007/s00367-006-0027-1

Siegle E, Asp NE (2007) Wave refraction and long shore transport patterns along the southern Santa Catarina Coast. Braz J Oceanogr 55(2):109–120

Siegle E, Schettini CAF, Klein AHF, Toldo EE Jr (2009) Hydrodynamics and suspended sediment transport in the Camboriú estuary—Brazil: pre jetty conditions. Braz J Oceanogr 57(2):123–135

Stark N, Wever TF (2009) Unravelling subtle details of expendable bottom penetrometers (XBP) deceleration profiles. Geo-Mar Lett 29:39–45. doi:10.1007/s00367-008-0119-1

Stech JL, Lorenzzetti JA (1992) The response of the South Brazil Bight to the passage of wintertime cold fronts. J Geophys Res 97 (C6):9507–9520

Teeter AM (1992) Evaluation of a new fluid mud survey system at field sites. US Army Eng Waterways Experiment Station, Dredging Res Tech Notes DRP-2-05

Teeter AM (1994) Fluid mud survey investigations at the Calcasieu Lake entrance channel, Florida. US Army Engineers Waterways Experiment Station, Dredging Res Tech Notes DRP-2-08

Tolman HL (1997) User manual and system documentation of WAVEWATCH-III version 1.15. NOAA/NWS/NCEP/OMB Tech Note 151

Tolman HL (1999) User manual and system documentation of WAVEWATCH-III version 1.18. NOAA/NWS/NCEP/OMB Tech Note 166

Traykovski P, Geyer WR, Irish JD, Lynch JF (2000) The role of wave-induced density-driven fluid mud flows for cross-shelf transport on the Eel River continental shelf. Cont Shelf Res 20:2113–2140

Truccolo EC, Franco D, Schettini CAF (2006) The low frequency sea-level oscillations in the northern coast of Santa Catarina, Brazil. J Coastal Res SI 39:547–552

van Rijn LC (1993) Principles of sediment transport in rivers, estuaries and coastal seas. Aqua, Amsterdam

Winterwerp JC (2005) Reducing harbor siltation. I. Methodology. J Waterway Port Coastal Ocean Eng 131(6):258–266

Winterwerp JC, van Kesteren WGM (2004) Introduction to the physics of cohesive sediment dynamics in the marine environment. Elsevier, New York

Wright LD, Nittrouer CA (1995) Dispersal of river sediments in coastal seas: six contrasting cases. Estuaries Coasts 18(3):494–508

Wright LD, Friedrichs CT, Kiom SC, Scully ME (2001) Effects of ambient currents and waves on gravity-driven sediment transport on continental shelves. Mar Geol 175:25–45

Zaleski AR, Schettini CAF (2006) Procedimentos para calibração de perfiladores acústicos de corrente por efeito Doppler para a determinação da concentração do material particulado em suspensão na água. Rev Brasileira Recursos Hídricos 11 (3):191–200